PHYSICAL REVIEW B **87**, 220408(R) (2013)

Three-dimensional artificial spin ice in nanostructured Co on an inverse opal-like lattice

A. A. Mistonov,[1] N. A. Grigoryeva,[1] A. V. Chumakova,[2] H. Eckerlebe,[3] N. A. Sapoletova,[4,5] K. S. Napolskii,[4] A. A. Eliseev,[4] D. Menzel,[6] and S. V. Grigoriev[1,2]

[1]*Faculty of Physics, Saint-Petersburg State University, 198504 Saint Petersburg, Russia*
[2]*Petersburg Nuclear Physics Institute, Gatchina, 188300 Saint Petersburg, Russia*
[3]*Helmholtz Zentrum Geestacht, 21502 Geesthacht, Germany*
[4]*Department of Materials Science, Moscow State University, 119992 Moscow, Russia*
[5]*Institute of General and Inorganic Chemistry, 119991 Moscow, Russia*
[6]*Institut für Physik der Kondensierten Materie, TU Braunschweig, 38106 Braunschweig, Germany*

(Received 3 January 2013; revised manuscript received 5 June 2013; published 28 June 2013)

The evolution of the magnetic structure for an inverse opal-like structure under an applied magnetic field is studied by small-angle neutron scattering. The samples were produced by filling the voids of an artificial opal film with Co. It is shown that the local configuration of magnetization is inhomogeneous over the basic element of the inverse opal-like lattice structure (IOLS) but follows its periodicity. Applying the "ice-rule" concept to the structure, we describe the local magnetization of this ferromagnetic three-dimensional lattice. We have developed a model of the remagnetization process predicting the occurrence of an unusual perpendicular component of the magnetization in the IOLS which is defined only by the direction and strength of the applied magnetic field.

DOI: 10.1103/PhysRevB.87.220408 PACS number(s): 75.50.Tt, 75.25.−j, 61.05.fm

The concept of frustrated magnetism has become very popular for complex crystal structures, where the competition between exchange interaction and crystal anisotropy results in the inability of the moment on a certain site to find an energy minimum. This description has originally been developed for triangular two-dimensional antiferromagnets.[1] Recently, the concept of magnetic frustration has expanded to three-dimensional (3D) systems, including the so-called "spin-ice" systems, where the Ising-like magnetic moments of rare-earth ions [Ho^{3+} (Ref. 2), Dy^{3+} (Ref. 3)] occupy lattice sites of corner-shared tetrahedrons and are magnetically frustrated due to anisotropy and ferromagnetic interactions.[4–7] The characteristic energies which govern the magnetic behavior of these systems are of the order of 0.1 meV (about 1 K on the temperature scale).

In the search for a way to increase the energy scale and, thus, the corresponding temperatures in frustrated systems, one comes across the magnetic nanomaterials.[8–13] The magnetic properties of a two-dimensional square lattice of isolated magnetic rods on a length scale of 1 μm have recently been studied.[8,9] The crossing of the magnetic rods was considered as a structural element of an "artificial spin ice," which is frustrated at room temperature.[10–12] Another artificial spin ice based on a continuous cobalt honeycomb network has even more complex phenomena, such as magnetic chirality in the spin ice giving rise to an anomalous or topological Hall effect.[13] Thus, the artificial spin ice can be a playground for physicists to study various phenomena associated with magnetic frustration. However, the majority of the artificial spin ices, being produced by lithography, are two dimensional.

In this Rapid Communication we focus on the magnetic properties of a three-dimensional network constructed by magnetic elements of size 400–500 nm, which form a face-centered-cubic (fcc) lattice defining an inverse opal-like structure (IOLS). Small-angle neutron-scattering (SANS) experiments have shown that the local configuration of the magnetization coincides with the spatial network of IOLS following the directions determined by the symmetry of the structure. Since, in analogy to the "spin-ice rule," the magnetic flux conservation law for the elements of the structure must be fulfilled, we have developed a model for the distribution of the magnetic moments within the IOLS. The scattering intensity predicted by the model is in qualitative agreement with the experimental data. Thus, we show that the magnetism in IOLS follows the ice-rule model, which predicts the occurrence of a magnetic component perpendicular to the applied magnetic field.

An inverse opal-like Co film has been prepared using the following templating technique:[14–17] First, polystyrene spheres with mean diameter of 540 nm form a colloidal crystalline face-centered-cubic template on top of a conductive substrate (polished Si single crystal, covered by the 10 nm Au layer) covering an area of 1 cm^2 with a thickness of 14 μm. Subsequently, the voids between the spheres are filled with Co via an electrochemical crystallization process. Finally, the microspheres are dissolved in toluene. It has been shown that the ferromagnetic behavior of such a structure is governed by the geometry of the network.[18–21] However, neither a detailed analysis of the magnetic properties has been done yet, nor has an appropriate model been suggested for this system so far.

Microradian x-ray diffraction has shown that the sample possesses fcc symmetry with a periodicity of 760 ± 10 nm.[20] A scanning electron microscopy (SEM) image of the sample surface is presented in Fig. 1, and a wider view of the (111) plane is shown in the inset of Fig. 1. The inverse OLS is built of unit elements consisting of three parts: two quasitetrahedra separated by a quasicube. They are connected by vertices along one of the four [111]-type axes. The surfaces of the cube and tetrahedra are concave resembling the voids between spheres. The projection of the unit element on the (111) plane is displayed in Fig. 1(b). The tetrahedra on the left and right sides of the cube are positioned at different depths in Fig. 1(a). They are denoted as TU (upper tetrahedron) and TD (lower tetrahedron). For an IOLS with the period of 760 nm one

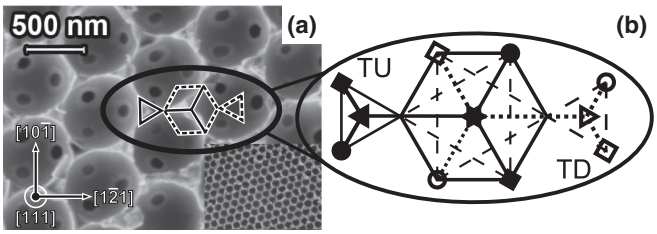

FIG. 1. Top view of the Co IOLS sample representing the (111) plane of the fcc structure (a). The unit element of IOLS consists of two tetrahedra connected by a cube (b).

can estimate that the cube has a volume of $\approx 220^3$ nm^3 and the tetrahedra have a volume of $\approx 120^3$ nm^3. The connecting "legs" have a length of $\approx$160 nm.

Neglecting the magnetocrystalline anisotropy of the material, we suppose that due to the shape anisotropy of the connecting "legs" the magnetic moments are aligned along the axes of the legs and, thus, considered as Ising-like spins. These connections define the easy axes of the local magnetization of the IOLS sample being along the four $\langle 111 \rangle$ directions.

The tetrahedra can be viewed as the point where the four vertices/legs of four different cubes are connected. To minimize the magnetic energy of the structure the magnetic flux is conserved in each tetrahedron following the so-called "ice rule", which is formulated for spin ice,[2,3] i.e., two moments point into and two moments point out of the tetrahedron. Such an ice rule should also hold for the cubes surrounded by eight tetrahedra in the IOLS. The ice rule acquires for IOLS a more generalized form: The net magnetic flux inside a tetrahedron or cube equals zero.

In the fully demagnetized state the IOLS is intrinsically frustrated similar to the model of the artificial spin ice.[8–12] We focus on the IOLS under an applied magnetic field when the frustration and degeneracy is lifted for certain directions of the field by favoring energetically local magnetic moments with a positive projection to the field direction.

Using the ice rule model one can estimate both the total magnetic energy of the IOLS and its average magnetization. Twelve of the 14 vertices present in one unit element are shared with the neighboring elements and, thus, doubly counted and labeled by the same symbols in Fig. 1(b). Therefore, for the magnetic structure based on IOLS the unit element is a combination of the four moments of the lower tetrahedron (TD) and the four moments of the upper tetrahedron (TU). The average magnetization is the sum of all eight moments of the unit element and corresponding magnetic energy given by

$$\mathbf{M} = M_0 \sum_{h,k,l=-1,1} \mathbf{m}_{[hkl]} \quad \text{and} \quad E = -\mathbf{MH} + E_{\text{ice rule}}, \tag{1}$$

where M_0 is the magnetic moment of one vertex, $\mathbf{H}$ is the magnetic field, and $\mathbf{m}$ is the magnetic moment. $E_{\text{ice rule}}$ denotes the energy of the magnetic flux inside the element, which is minimal, when the ice rule is fulfilled for both tetrahedra. The situation when three moments are directed towards each other opposite to the fourth moment at the tetrahedron "crossroads," or vice versa, is less favorable and the energy $E_{\text{ice rule}}$ increases. The most unfavorable configuration

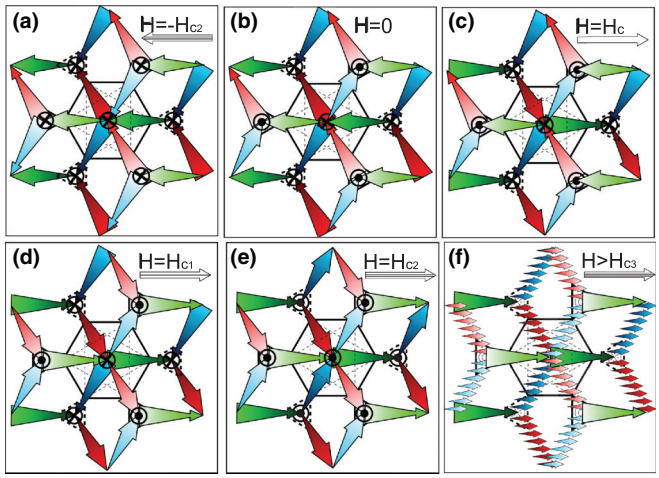

FIG. 2. (Color online) Magnetization distribution in IOLS for different stages of the remagnetization process: at $H \sim -H_{c2}$ (a), at $H = 0$ (b), at $H = H_c$ (c), at $H = H_{c1}$ (d), at $H = H_{c2}$ (e), and at $H > H_{c3}$ (f). The Ising-like magnetic moments (labled with arrows) are oriented along the $\langle 111 \rangle$ axes. Moments in the upper plane are light-colored.

arises when all four moments point towards or away from each other at the crossroads.

In order to gain insight into the remagnetization process the magnetic states of the IOLS at different magnetic fields have to be considered. These states in the magnetic field applied along the [1$\bar{2}$1] axis are presented in Fig. 2.

It is convenient to consider one layer of the (111) plane of the structure. Each layer is connected to the neighboring ones only via "legs" in the [111] direction perpendicular to the layer plane and the magnetic field. The moments along the $\langle 111 \rangle$ axes can be divided into four magnetic subsystems, which are represented by arrows in Fig. 2, and connect the central cube via eight vertices with the neighboring tetrahedra. When the magnetic field is applied in the (111) plane, the out-of-plane moments along [111] seem to be degenerate. However, as will be shown below, due to the ice rule this degeneracy is lifted.

The remagnetization scenario starts in a relatively large field $H \sim -H_{c2}$ [Fig. 2(a)]. The magnetic moments have positive projections with respect to the field direction and are oriented along the three [$\bar{1}$11], [1$\bar{1}$1], and [11$\bar{1}$] axes. In such a configuration, one magnetic moment points towards the upper tetrahedron, whereas two moments point away from the tetrahedron. According to the ice rule the fourth moment perpendicular to the plane should also point towards the upper tetrahedron (downwards). For the lower tetrahedron the situation is opposite, i.e., two magnetic moments point towards and one moment points away from the tetrahedron. The fourth moment is expected to point away (downwards) similar to the upper tetrahedron. Therefore, the sample has an additional magnetization component, which is perpendicular to the (111) plane pointing downwards and, thus, perpendicular to the negative applied field.

In zero magnetic field the sample is remanently magnetized. In a small and negative field $|H| < |H_c|$ the moment along either the [$\bar{1}$11] or [11$\bar{1}$] axis will most likely reorient, since it has the largest angle (62°) with respect to the field [Fig. 2(b)]. In order to satisfy the ice rule this flip takes place

TABLE I. Values of the magnetization components parallel and perpendicular to the field at different stages of the reorientation process which correspond to the panels of Fig. 2.

Stage	$M_{\parallel}$	$M_{\perp}$
a	$-2M_0(\cos 19^\circ + 2\cos 62^\circ)$	$-2M_0(1+\cos 70^\circ)$
b	$-2M_0(\cos 19^\circ + \cos 62^\circ)$	0
c	0	0
d	$2M_0(\cos 19^\circ + \cos 62^\circ)$	0
e	$2M_0(\cos 19^\circ + 2\cos 62^\circ)$	$2M_0(1+\cos 70^\circ)$
f	$8M_0$	0

in combination with the reorientation of the moment along the [111] direction. In a second step the other two local moments flip. In a small but positive field $H < H_c$ the moment along the $[1\bar{1}1]$ axis will most likely reorient, since it has the smallest angle (19°) with respect to the field. Herewith, each magnetic subsystem reorientates at different critical fields $H_{c(i)}$. At $H = H_c$ half of the moments are reoriented and the sample becomes demagnetized, i.e., **M** is equal to zero [Fig. 2(c)]. Most likely the process is driven by an avalanche effect.

In the field range $H > H_c$ the pairwise reorientation of the local moments continues. This reorientation process of the local moments is completed at $H = H_{c2}$, where all local moments in the tetrahedra are pointing opposite to the situation at the starting field $H = -H_{c2}$. The perpendicular component of the magnetization is pointing up [Fig. 2(e)].

This magnetization state is stable over a large field range up to $H = H_{c3}$, above which the magnetic moments tend to rotate towards the magnetic field direction [Fig. 2(f)]. In this state the magnetic field dominates the anisotropy of IOLS, and the ice rule is not satisfied anymore. The process of reorientation covers a large field range and is completed at a high magnetic field $H > 1.2$ T.

The average magnetization parallel and perpendicular to the field direction ($M_{\parallel}$ and $M_{\perp}$) can be calculated for each magnetization stage by using Eqs. (1) and Fig. 2. However, it is necessary to take into account, that states (b), (c), and (d) in Fig. 2 are frustrated and all variants of the magnetization distribution should be considered and averaged. Calculated values of the magnetization components are presented in Table I.

To prove the model, we performed SANS experiments at the SANS-2 in Geesthacht (Germany). A neutron beam with a wavelength $\lambda = 1.2$ nm, a bandwidth $\Delta\lambda/\lambda = 0.1$, and a divergence $\eta = 1.5$ mrad was used. The scattered neutrons were detected by a position sensitive detector with a resolution of 256 × 256 pixels, each of 2.2 × 2.2 mm^2 size. The detector-to-sample distance was set at 21.5 meters such that the Q range covers 5–70 μm^{-1} with a step of 0.5 μm^{-1}. Accounting for the small sample thickness and highest possible resolution required the experiment was carried out at the limit of abilities of the modern SANS instruments. The cobalt IOLS films were oriented perpendicular to the incident neutron beam. An external magnetic field H up to 1.2 T was applied in the plane of the film which was decisive for this experiment since it has revealed a magnetized state of the sample that was not reached in the previous work.[20] The neutron diffraction patterns recorded in the experiments consisted of several

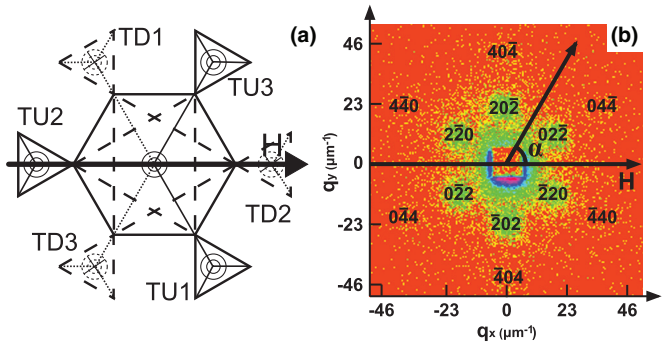

FIG. 3. (Color online) (a) Projection of an idealized basic element of the IOLS on the (111) plane with attached tetrahedra of four neighboring elements. (b) Neutron diffraction patterns for Co IOLS with the magnetic field $H = 294$ mT along the $[1\bar{2}1]$ axis. The Miller indices of the reflections correspond to the fcc structure with the lattice constant of $a_0 = 760 \pm 10$ nm.

clearly resolved sets of hexagonally arranged reflexes (Fig. 3). The measurements were performed at 300 K.

All reflections of the 202 type visible in Fig. 3(b) were divided into subgroups: $20\bar{2}$ and $\bar{2}02$ reflections with an angle α of 90° between **Q** and **H**; and $02\bar{2}$, $0\bar{2}2$, $2\bar{2}0$, and $\bar{2}20$ reflections with an angle α of 30° between **Q** and **H**. The intensities of these magnetic reflections were averaged over the subgroups in order to improve the statistics.

The intensity I_M of nonpolarized neutron scattering for magnetic structures with a large period can be described by the equations

$$I_M(\mathbf{Q}) \sim |A_m \mathbf{m}_{\perp\mathbf{q}} \mathcal{S}(\mathbf{Q}) F(Q)|^2, \quad \mathbf{m}_{\perp\mathbf{q}} = \mathbf{m} - (\mathbf{qm})\mathbf{q} \qquad (2)$$

with the unit vectors **m** and **q** of the magnetization **M** and the momentum transfer **Q**. A_m is the amplitude of the magnetic scattering, $S(\mathbf{q})$ is the structure factor, and $F(q)$ is the form factor. The magnetic field dependence of I_M for the Co IOLS is presented in Figs. 4(a) and 4(b) and is accompanied by the magnetization curve taken from the sample in the same field-to-sample geometry [Fig. 4(c)].

In the model described above the experimental data can be easily interpreted. The magnetic intensity I_M is proportional to the volume of the scattering element magnetized in the direction $[hkl]$ ($V_{[hkl]}$), which is considered equal for the four directions along the ⟨111⟩ axes. It is proportional to the squared magnetization $|\mathbf{m}_{\perp\mathbf{q}}|^2$ projected to the plane normal to the scattering vector **Q** [Eq. (2)]. We also introduce the proportionality factor $a_i(H_{c(i)})$, which is equal to 0, when the subsystem is nonmagnetized, and equal to 1, when it is magnetized. $H_{c(i)}$ is the threshold field of these subsystems, where the magnetization changes from 0 to 1.

$$I_M(Q) \sim \sum_i a_i(H_{ci}) m_i^2 \cos^2(\angle \mathbf{m}_{\perp\mathbf{q},\mathbf{i}}, \mathbf{m_i}). \qquad (3)$$

For example, intensity $I_M(20\bar{2})$ is dominated by contributions from the subsystems aligned along $[\bar{1}1\bar{1}]$ and [111], and contributions from the other two subsystems along the $[\bar{1}11]$ and $[11\bar{1}]$ are reduced by a factor of $\cos^2 55^\circ \approx 0.328$.

The fact that all four moment subsystems are magnetized differently and saturate at different values of the applied magnetic field $H_{c(1,2,3,4)}$ is observed in the field dependence of

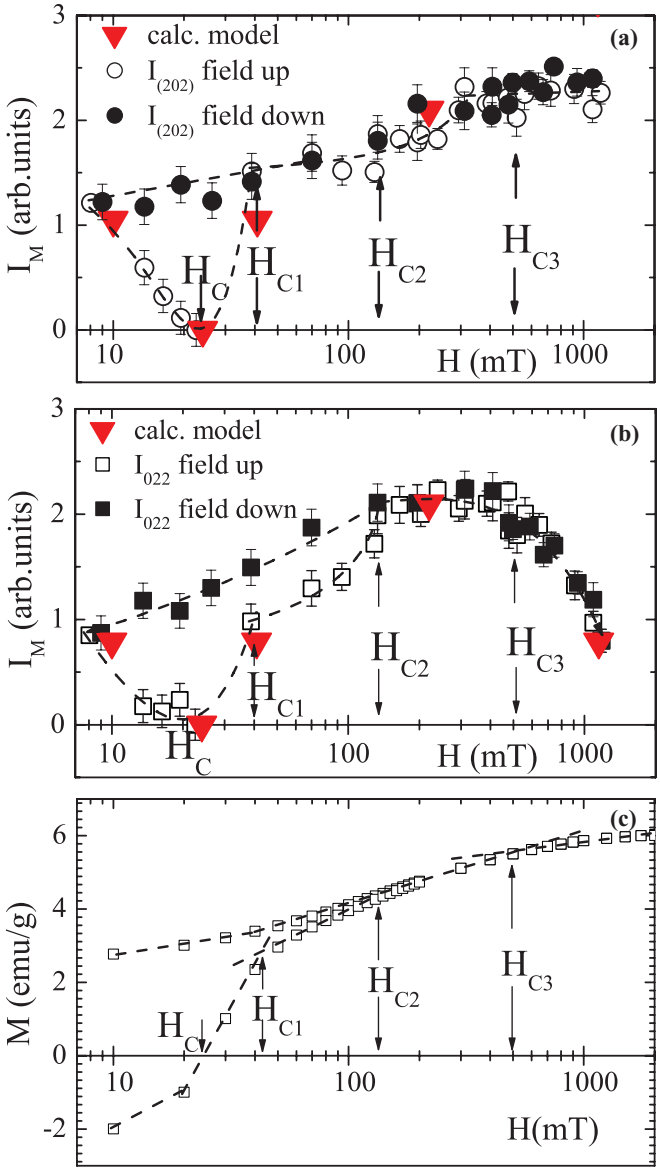

FIG. 4. (Color online) Field dependence of the magnetic intensity I_M of neutron scattering on Co IOLS with $\mathbf{H} \parallel [\bar{1}2\bar{1}]$ (a) at $\mathbf{Q}_{20\bar{2}} \perp \mathbf{H}$, (b) at $\mathbf{Q}_{02\bar{2}}$ inclined at 30° with respect to the field $\mathbf{H}$, and (c) of the total magnetization.

the Bragg intensity of the reflections $I_M(20\bar{2})$ and $I_M(02\bar{2})$ in Figs. 4(a) and 4(b), respectively. The corresponding theoretical points are also presented. One can distinguish three specific fields in the range from 0 to 1.2 T. The coercive field $H_c =$ 24 mT is clearly established as the minimum of the intensity in both dependencies $I_M(20\bar{2})(H)$ and $I_M(02\bar{2})(H)$. At $H_{c1} =$ 40 mT a steep increase of $I_M(20\bar{2})(H)$ and $I_M(02\bar{2})(H)$ is observed. The critical field $H_{c2} = 140$ mT, where the intensity $I_M(20\bar{2})$ changes slightly but abruptly, coincides with the field where the intensity $I_M(02\bar{2})$ reaches its maximum and saturates. $H_{c3} = 400$ mT is a further critical field, where the intensity $I_M(20\bar{2})$ undergoes another small but abrupt change, while the intensity $I_M(02\bar{2})$ starts to decrease smoothly. This decrease of $I_M(02\bar{2})$ is observed up to the highest measured field $H = 1.2$ T. The intensity $I_M(20\bar{2})$ remains unchanged in the range from H_{c3} to 1.2 T. The magnetization measurements performed using a superconducting quantum interference device magnetometer confirmed the presence of these characteristic fields: H_c, H_{c1}, H_{c2}, and H_{c3} [see Fig. 4(c)].

Obviously the theoretical points are in good qualitative agreement with the experimental data, but some differences should be noted. First, the calculated point at H_{c1} is lower than both intensities in the experiment. This is due to the fact that our calculations describe only the consequent flipping of two types of magnetic moment pairs, while it can occur contemporaneously. Secondly, the last theoretical point is too high for $I_M(20\bar{2})$ (out of plot). This can be explained by the demagnetization occurring inside structural nanoelements in high magnetic fields.

We note that the value of the perpendicular component of the magnetization depends strongly on the orientation of the film in the magnetic field. When the field is applied along the $\langle 11\bar{2}\rangle$ axes, the strong perpendicular component of the magnetization points down. It decreases to zero, when the field is along $\langle 10\bar{1}\rangle$, and points up, when the field is along the $\langle 2\bar{1}\bar{1}\rangle$ axis. It changes with the period of 120°, which is determined by the threefold symmetry of the IOLS in the (111) plane. Obviously even more complex and interesting situations may occur when the magnetic field is applied out of the (111) plane.

It is interesting to refer to the similar phenomenology in spin-ice systems.[22–24] For example, highly featured hysteresis loops and avalanchelike jumps of the magnetization are reported in Refs. 22 and 23, and a perpendicular magnetic moment controlled by a longitudinal field applied along [112] is observed in Ref. 24. These comparisons and analogies give additional credibility to the model proposed in this Rapid Communication. In conclusion, we note that the applicability of the ice-rule concept to this nanoscale system results first in the change of the macroscopic properties of the magnetic network of the IOLS: A magnetization component perpendicular to the applied magnetic field should appear, which is comparable to the component parallel to the field. In addition, our concept introduces the magnetic network of IOLS as a 3D frustrated magnetic system at room temperature and, more generally, as a fascinating object for both fundamental studies and applications.

We thank the Medical Research Council "Nanotechnology" for the SEM investigations and the Helmholtz Zentrum Geestacht for hospitality and financial support. This work is supported in part by the DAAD in the framework of the Mikhail Lomonosov II program, by the Russian Foundation for Basic Research (Project No. 12-02-12066) and the RF Program (Project No. 2012-1.2.1-12-000-1010-051).

[1] G. H. Wannier, Phys. Rev. **79**, 357 (1950).

[2] M. J. Harris, S. T. Bramwell, D. F. McMorrow, T. Zeiske, and K. W. Godfrey, Phys. Rev. Lett. **79**, 2554 (1997).

[3] A. P. Ramirez, A. Hayashi, R. J. Cava, R. Siddharthan, and B. S. Shastry, Nature (London) **399**, 333 (1999).

[4] L. Balents, Nature (London) **464**, 199 (2010).

[5]Christopher L. Henley, Annu. Rev. Condens. Matter Phys. **1**, 179 (2010).

[6]Michel J. P. Gingras, in *Introduction to Frustrated Magnetism: Materials, Experiments, Theory*, edited by Claudine Lacroix, Philippe Mendels, and Fridiric Mila, Springer Series in Solid-State Sciences, Vol 164 (Springer, New York, 2011), p. 679.

[7]C. Castelnovo, R. Moessner, and S. L. Sondhi, Annu. Rev. Condens. Matter Phys. **3**, 35 (2012).

[8]R. F. Wang, C. Nisoli, R. S. Freitas, J. Li, W. McConville, B. J. Cooley, M. S. Lund, N. Samarth, C. Leighton, V. H. Crespi, and P. Schiffer, Nature (London) **439**, 303 (2006).

[9]P. E. Lammert, X. Ke, J. Li, C. Nisoli, D. M. Garand, V. H. Crespi, and P. Schiffer, Nat. Phys. **6**, 786 (2010).

[10]J. P. Morgan, A. Stein, S. Langridge, and C. H. Marrows, Nat. Phys. **7**, 75 (2011).

[11]J. Cumings, Nat. Phys. **7**, 7 (2011).

[12]V. Kapaklis, U. B. Arnalds, A. Harman-Clarke, E. Th. Papaioannou, M. Karimipour, P. Korelis, A. Taroni, P. C. W. Holdsworth, S. T. Bramwell, and B. Hjörvarsson, New J. Phys. **14**, 035009 (2012).

[13]W. R. Branford, S. Ladak, D. E. Read, K. Zeissler, and L. F. Cohen, Science **335**, 1597 (2012).

[14]A. A. Grunin, N. A. Sapoletova, K. S. Napolskii, A. A. Eliseev, and A. A. Fedyanin, J. Appl. Phys. **111**, 07A948 (2012).

[15]L. Xu, L. D. Tung, L. Spinu, A. A. Zakhidov, R. H. Baughman, and J. B. Wiley, Adv. Mater. **15**, 1562 (2003).

[16]P. N. Bartlett, P. R. Birkin, and M. A. Ghanem, Chem. Commun. **17**, 1671 (2000).

[17]L. Xu, W. L. Zhou, C. Frommen, R. H. Baughman, A. A. Zakhidov, L. Malkinski, J.-Q. Wang, and J. B. Wiley, Chem. Commun. **12**, 997 (2000).

[18]A. A. Zhukov, A. V. Goncharov, P. A. de Groot, A. G. Mohamed, P. N. Bartlett, R. Boardman, H. Fangohr, V. Novosad, and G. Karapetrov, Appl. Phys. Lett. **88**, 062511 (2006).

[19]S. V. Grigoriev, K. S. Napolskii, N. A. Grigoryeva, A. V. Vasilieva, A. A. Mistonov, D. Yu. Chernyshov, A. V. Petukhov, D. V. Belov, A. A. Eliseev, A. V. Lukashin, Yu. D. Tretyakov, A. S. Sinitskii, and H. Eckerlebe, Phys. Rev. B **79**, 045123 (2009).

[20]N. A. Grigoryeva, A. A. Mistonov, K. S. Napolskii, N. A. Sapoletova, A. A. Eliseev, W. Bouwman, D. V. Byelov, A. V. Petukhov, D. Yu. Chernyshov, H. Eckerlebe, A. V. Vasilieva, and S. V. Grigoriev, Phys. Rev. B **84**, 064405 (2011).

[21]M. V. Sapozhnikov, O. L. Ermolaeva, B. G. Gribkov, I. M. Nefedov, I. R. Karetnikova, S. A. Gusev, V. V. Rogov, B. B. Troitskii, and L. V. Khokhlova, Phys. Rev. B **85**, 054402 (2012).

[22]D. Slobinsky, C. Castelnovo, R. A. Borzi, A. S. Gibbs, A. P. Mackenzie, R. Moessner, and S. A. Grigera, Phys. Rev. Lett. **105**, 267205 (2010).

[23]T. Fennell, O. A. Petrenko, B. Fak, J. S. Gardner, S. T. Bramwell, and B. Ouladdiaf, Phys. Rev. B **72**, 224411 (2005).

[24]J. P. C. Ruff, R. G. Melko, and M. J. P. Gingras, Phys. Rev. Lett. **95**, 097202 (2005).